ACS APPLIED MATERIALS & INTERFACES

RESEARCH ARTICLE

www.acsami.org

Carbon Aerogel Composites Prepared by Ambient Drying and Using Oxidized Polyacrylonitrile Fibers as Reinforcements

Junzong Feng,[†] Changrui Zhang,[†] Jian Feng,[*,†] Yonggang Jiang,[†] and Nan Zhao[‡]

[†]Key Lab of Advanced Ceramic Fibers and Composites, College of Aerospace and Materials Engineering, National University of Defense Technology, 109 De Ya Rd, Changsha, Hunan, 410073, China

[‡]Northwest Institute of Nuclear Technology, 28 Ping Yu Rd, Xi'an, Shanxi, 710024, China

Supporting Information

ABSTRACT: Carbon fiber-reinforced carbon aerogel composites (C/CAs) for thermal insulators were prepared by copyrolysis of resorcinol-formaldehyde (RF) aerogels reinforced by oxidized polyacrylonitrile (PAN) fiber felts. The RF aerogel composites were obtained by impregnating PAN fiber felts with RF sols, then aging, ethanol exchanging, and drying at ambient pressure. Upon carbonization, the PAN fibers shrink with the RF aerogels, thus reducing the difference of shrinkage rates between the fiber reinforcements and the aerogel matrices, and resulting in C/CAs without any obvious cracks. The three point bend strength of the C/CAs is 7.1 ± 1.7 MPa, and the thermal conductivity is 0.328 W m^{-1} K^{-1} at 300 °C in air. These composites can be used as high-temperature thermal insulators (in inert atmospheres or vacuum) or supports for phase change materials in thermal protection system.

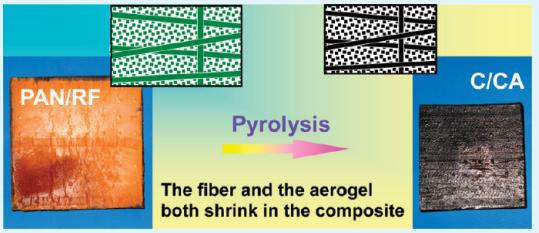

KEYWORDS: carbon aerogels, carbon−carbon composites, polyacrylonitrile fibers, ambient drying, residual stress, thermal conductivity, bend strength

1. INTRODUCTION

High-temperature thermal insulators with high thermal insulation values and high mechanical strength are required for the thermal protection systems of the hypersonic vehicles (Mach number as high as 12),[1] which endured high heat flux and ultrahigh temperature.[2] Aerogels are nanoporous solid materials with high surface area, high porosity, and low density.[3] Due to their unique nanometer network and nanoporous structure, which suppress the gaseous thermal conduction significantly, aerogels exhibit very low thermal conductivity, e.g., 0.012 W m^{-1} K^{-1} at room temperature for resorcinol-formaldehyde (RF) aerogels,[4] and they are excellent thermal insulators used in aerospace.[5] In the many aerogels, with a variety of chemical compositions ranging from inorganic oxides to polymers that have been explored to date,[6−16] carbon aerogels (CAs) have the highest thermal stability and can maintain their mesoporous structure at a high temperature even exceed 2000 °C in an inert atmosphere.[17] In addition, CAs exhibit much higher specific extinction coefficients than other kinds of aerogels, thus the radiative thermal conduction, which is the dominating component of heat transfer at high temperature, is very low.[18] It is also well-known that the carbon materials (foam, fiber felt, and rigid carbon bonded carbon fiber tile) have been widely used as high temperature thermal insulators or thermal structures.[19] Therefore, CA is one of the most promising materials for high-temperature thermal insulators in thermal protection system,[20] especially for the hypersonic vehicles or the space vehicles that endured high heat flux and high temperature. Of course, the CAs must be coated with antioxidation coatings when they are used in air because they may be oxdized at above about 500 °C in the presence of oxygen.

Similar to silica aerogels, CAs are brittle and fragile, and they collapse easily. So it is difficult to prepare the CA in a large-scale industrial setting. There has been a lot of excellent work on reinforcing the silica aerogels by cross-linked polymers between the necks of the particles of the network chains,[21−23] it can significantly improve the strength by as much as 2 orders of magnitude while only doubling the density over those of native or nonreinforced aerogels.[24,25] However, this cross-linking method is inappropriate for the CAs because it has been found that pyrolysis under inert atmosphere of polyurea-cross-linked RF aerogels yields macroporous carbons,[26] whereas it is well-known that pyrolysis of native RF aerogels leads to typical mesoporous carbon aerogels. At the early stages of carbonization (200−250 °C) polyurea is detached chemically from the RF skeletal framework above its melting point (123 °C), and by melting causes local framework collapse with creation of macropores surrounded by xerogel-like walls.

Reinforcing the brittle ceramics with fibers to fabricate composites such as C/C,[27] C/SiC,[28,29] and SiC/SiC[30,31] is an effective way to improve the mechanical properties. To overcome the similar brittleness for CAs, many attempts to strengthen the

Received: September 21, 2011
Accepted: November 2, 2011
Published: November 02, 2011

ACS Publications © 2011 American Chemical Society

dx.doi.org/10.1021/am201287a | ACS Appl. Mater. Interfaces 2011, 3, 4796–4803

gel skeletons by reinforcing them with carbon fibers,[32−34] carbon nanotubes,[35−38] and ceramic fibers[39] have been explored. Unfortunately, these hard reinforcements barely shrink, whereas the CAs are derived from carbonizing organic aerogels, they exhibit large linear shrinkage of 20% or higher.[40,41] Thus the different shrinkage rates between the reinforcements and the CA matrices will lead to large residual stresses and then lead to large cracks. The cracks in the composites reinforced by hard carbon fibers can be as large as 0.5 mm.[33] These large cracks may be detrimental for the CAs using as thermal insulators, because they may increase the gaseous thermal conductivity. In addition, overlarge cracks may decrease the mechanical strength of the composites.

To reduce the cracks and improve the methods that using inorganic fibers or tubes as hard reinforcements, in this paper we introduce a new concept that using oxidized polyacrylonitrile (PAN) fibers as soft reinforcements to prepare an organic fiber-reinforced organic aerogel composite first, and then carbonizing to form a carbon fiber-reinforced carbon aerogel composite (C/CA). The organic PAN fiber felts are directly impregnated by RF sols. Afterward, the RF gels are synthesized in the void space between the PAN fibers. After drying at ambient pressure, the organic PAN/RF aerogel composites are obtained. Upon carbonization, the PAN fibers shrink with the RF aerogels to form carbon composites, thus reducing the difference of shrinkage rates between the fiber reinforcements and the aerogel matrices, and results in CA composites with improved mechanical properties and without any obvious cracks.

There are some reasons for why we used oxidized PAN fiber felts instead of native PAN fiber felts as the organic fiber reinforcements. The oxidative stabilization is an essential step in the production of PAN-based carbon fibers.[42,43] This process is necessary to cross-link PAN chains and prepare a structure that can withstand the rigors of high-temperature processing before carbonization, lack of or nonoptimized oxidative stabilization can also lead to excessive weight loss during subsequent carbonization, and to carbon fibers with inferior properties. Oxidative stabilization is normally performed at 200−300 °C in the presence of air and the PAN fiber is prestressed to a constant tension (to improving preferred orientation and mechanical properties). However, if we use PAN fiber directly, first, in the composite we can not put tension on the PAN fibers, and second, we can not oxidize the PAN/RF composites because we have found that the RF aerogel would smoke and catch fire above 120 °C in air; the same phenomena has also been found for phenolic-furfural aerogels.[44]

We used RF as carbon precursors because the RF aerogels need no oxidation before carbonization, whereas other organic aerogels like polyurethanes,[45] polyureas,[46] polybenzoxazines,[47,48] and PAN[49] need oxidation. The oxidation is an exothermic process. When the organic aerogel monoliths are small, it is easy to release the heat caused by oxidation, in the case of the references mentioned above. But one of the purposes of our work is to fabricate the C/CAs in large scale settings, which are required in the practical thermal insulator applications. The organic composites we prepared are as thick as 50 mm. They are really thick and it is difficult to oxidize them and to release the heat out of the bulk, if the organic aerogels need to be oxidized before carbonization.

To gel the RF, there are two sorts of catalyst: base and acid. The acid-catalyzed methods can really reduce the gelation time. But in our case, because in the drying process the fiber reinforcements do not shrink, there is lower shrinkage and higher strength for the RF aerogel matrices, fewer cracks, and higher strength for the composites. And the narrower the pore size for the aerogels, the lower the thermal conductivity for the composites. However, the high concentration HCl-catalyst RF aerogels ($R/C_{HCl} = 0.55$),[50] using water as solvent and dried at ambient pressure, exhibit very low specific surface area ($\leq 14.19\ m^2/g$), and they are weak and can be easily broken in hand by soft pressure, which is not possible with the Na_2CO_3-catalyst RF aerogels with the same density ($0.41\ g\ cm^{-3}$). When using HCl as catalyst and CH_3CN as solvent, the obtained gels shrink largely ($\geq 29\%$) even dried with supercritical CO_2.[51] When using hydrated metal ions to catalyze gelation of RF, the linear shrinkage dried at ambient pressure is as large as 47.1−64.4%.[52]

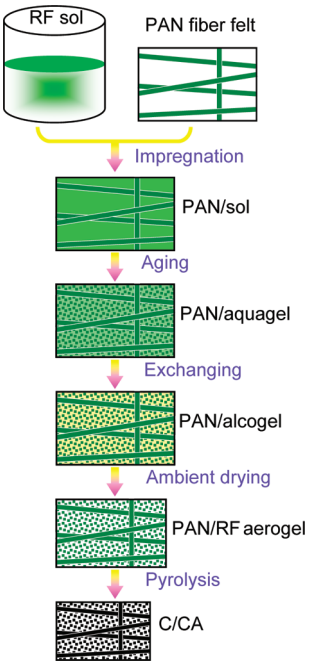

Figure 1. Flowchart of the synthesizing process.

The structure of base-catalyst (Na_2CO_3) RF gels can be easily tailored in a wide range by varying the processing conditions (monomer concentrations and R/C values).[41] Also, the surface area in based-catalyzed aerogels is relatively high compared to acid-catalyzed RF aerogels.[53] Therefore, we take advantage of this flexibility of Na_2CO_3-catalyst method to prepare a suitable gel to reduce density as low as possible, and shrinkage and pore size as small as possible for the matrices in the composites.

2. EXPERIMENTAL SECTION

2.1. Materials. Resorcinol (R), formaldehyde (F), sodium carbonate (C), and ethanol were purchased from Shanghai National Chemical Co. (China), deionized water (W) was obtained from Huihong Chemical Co. (China). The oxidized PAN fiber felts (preoxidized temperature 260 °C) were purchased from Nantong Senyou Carbon Fiber Co. (China). All of the chemical reagents were used as received.

2.2. Preparation. The synthesizing process is shown in Figure 1. The RF sols were synthesized by using R and F as precursors, W as solvent, and C as catalyst. The molar ratio of F/R was 2, the ratios of R/C and W/R were set to be 250−2000 and 1−26, respectively. The oxidized PAN fiber felts were used as reinforcements. The fiber orientation in the felt is anisotropic, most of the fibers are along the felt plane (in-plane direction), and only a few needled fibers are along the perpendicular direction of the felt plane (through-plane direction). Single fiber felt is about 15 mm thick and its apparent density is about $0.1\ g\ cm^{-3}$. Several felts

were piled together and two stainless steel plates were used to press them to obtain a desired thickness (12−50 mm) and a desired apparent density (0.12 g cm^{-3}). After keeping the RF sols at room temperature for 1 day, the fixed PAN fiber felts were impregnated with the RF sols under vacuum. Then the PAN fiber felts containing the RF sols were placed in 50 °C water bath for 1 day, and then at 95 °C for 2 days. The cured PAN/RF aquagel composites were soaked in ethanol for 7 days, with exchanging the ethanol one time for each day. Then the obtained PAN/RF alcogel composites were placed in an oven, and dried in air at 50 °C for 3 days and at 100 °C for 1 day (do not dry them at above 120 °C, or they may catch fire). The obtained PAN/RF aerogel composites were carbonized to form C/CAs at 1200 °C for 1 h under a flowing nitrogen atmosphere (200 mL min^{-1}). The composites both shrank in the ambient drying and the pyrolysis processes. For comparison, hard carbon fibers and mullite fibers (Al_2O_3−SiO_2) were also used as hard reinforcements and impregnated with the RF sols to prepared CA composites as the same procedure of the C/CAs from PAN fiber reinforcements to investigate their cracks and microstructure. Pure PAN fiber felts and pure RF aerogels were also carbonized as the pyrolysis procedure of the PAN/RF aerogel composites to measure their shrinkage.

2.3. Characterization. The linear shrinkage of the samples was calculated from the dimensions of the samples before and after ambient drying, or carbonization. The bulk density (ρ) was obtained by measuring the volume and the weight of the aerogels or the composites. The porosity was calculated by $(1 - \rho/\rho_s) \times 100\%$. ρ_s is the skeletal density, they are 1.55 and 2.19 g cm^{-3} for RF and carbon aerogels, respectively.[54] Nitrogen sorption measurements were performed to obtain pore properties such as specific surface area and specific pore volume with a QuadraSorb SI (Quantachrome, USA) analyzer. The desorption branches were used for the Barrett−Joyner−Halenda (BJH) calculation. The microstructure of the pure CAs and the C/CAs were investigated by a Hitachi S4800 scanning electron microscope (SEM) after coating the samples with a thin platinum layer. The pure CAs and the composites were cut into disk-shape with diameters of 12.7 mm and thicknesses of approximately 1.6 mm, and the thermal diffusivities in the through-plane direction of the samples (without any coatings) were determined by laser flash method using a Netzsch LFA 447 apparatus in air.[55,56] The Cowan method was selected to correct the diffusivity measurements with respect to heat losses. The effective thermal conductivity (λ_{eff}) was obtained according to eq 1 from the thermal diffusivity α, with a known specific heat capacity c_p and sample density ρ.[57]

$$\lambda_{eff} = \alpha(T)\rho c_p(T) \quad (1)$$

T is the temperature at which the measurement is performed. Literature values of specific heat capacity c_p were used.[57]

The bend strengths of the pure CAs and the C/CAs were tested by three point bending measurement with sample dimensions of 50 × 5 × 4 mm^3 and a span of 40 mm, using a WDW model 100 test machine (Changchun Machine Co., China) with a 1 kN load cell. The crosshead rate was 0.5 mm min^{-1}. Five specimens for each kind of sample were used.

3. RESULTS AND DISCUSSION

3.1. Effects of W/R and R/C Ratios on the Structural Properties of the RF Aerogels in the Drying Process. Compared to the conventional supercritical drying, which is expensive and time-consuming, the ambient drying of our PAN/RF gels is cheaper and safer.[58] And another important advantage for the ambient drying is that large samples can be easily dried and prepared. For supercritical drying, the sample dimension will be limited by the dimension of the autoclave that used to carry out the drying. Therefore, this ambient drying method makes the C/CAs of even greater interest as cheaper and easier for industrial

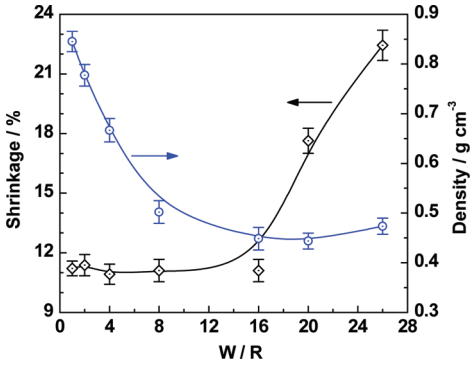

Figure 2. Shrinkage and density of RF aerogels prepared by different W/R ratios during the ambient drying process. The R/C ratio is kept constant as 1000.

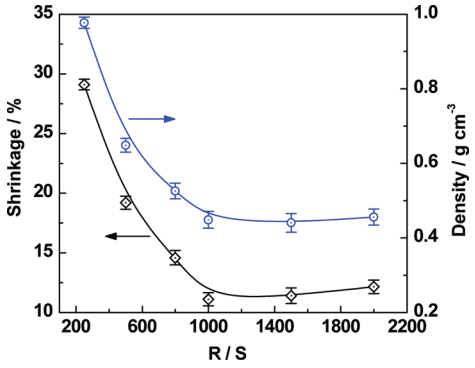

Figure 3. Shrinkage and density of RF aerogels prepared by different R/C ratios during the ambient drying process. The W/R ratio is kept constant as 16.

production. Lots of papers have described the ambient drying for aerogels,[13,32,50,58−63] and have concluded that the shrinkage during the drying process is affected by the pore size and the network strength of the gels, which are related to the molar ratios of the R/C and the W/R used in the preparation of the RF sols. However, in our special case, not only small pore size (for low gaseous conductivity) but also small shrinkage (for reducing cracks) are desired, and therefore, we must investigate the effects of R/C and W/R values on the shrinkage and the porosities in our experiments to get small shrinkage first and then to reduce the pore size by decreasing R/C values as low as possible. So we prepared RF aerogels with different molar ratios of R/C and W/R, and investigated their shrinkage before preparing the composites. The shrinkage and the densities of the RF aerogels prepared by different W/R ratios are shown in Figure 2. The R/C ratios are kept constant as 1000. It can be seen that, when the W/R ratios are lower than 16, the RF aerogels exhibit constant and mild shrinkage of approximately 11.0%. When the W/R ratios are higher than 16, the shrinkage increases sharply with increasing the W/R ratio, the reason is the weak skeleton structure resulted from the high W/R ratio (low reactant concentration). The densities of the RF aerogels change mildly when the W/R ratios are higher than 16, the reason is the integration of lower reactant concentration in the gel and higher shrinkage during the ambient drying.

Figure 3 shows the shrinkage and densities of the RF aerogels prepared by different R/C ratios during the ambient drying

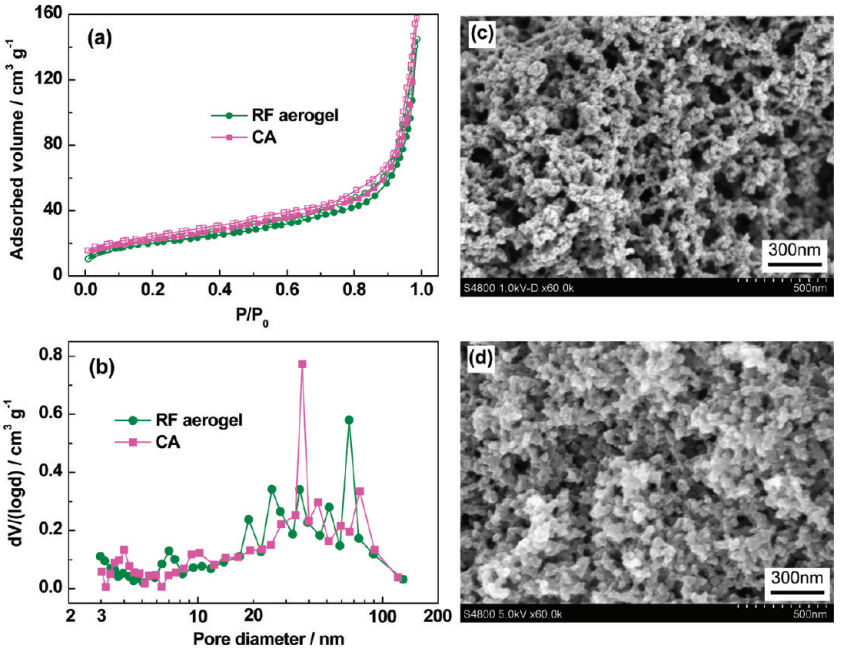

Figure 4. (a) Nitrogen sorption isotherm and (b) BJH pore size distribution of the RF aerogel and CA. SEM images of the (c) RF aerogel and (d) CA.

Table 1. Textural Properties of the RF Aerogel and the Related CA Prepared by R/C = 1000 and W/R = 16

material	density (g cm^{-3})	porosity (%)	S_{BET} [a] (m^2 g^{-1})	S_{mes} [b] (m^2 g^{-1})	S_{mic} [c] (m^2 g^{-1})	V_{Pore} [d] (cm^3 g^{-1})	D_{pore} [e] (nm)
RF aerogel	0.449	71.0	159.6	159.6	0	0.22	66
CA	0.446	79.6	168.0	114.6	53.4	0.24	37

[a] BET specific surface area. [b] Mesoporous surface area. [c] Microporous surface area. [d] Pore volume. [e] Pore diameter at the peak of the BJH distribution curve.

process. The W/R ratios are kept constant as 16. It can be seen that, when the R/C ratios are lower than 1000, the shrinkage increases sharply with decreasing the R/C ratio, the reason may be the larger capillary tensions resulted from narrower pore size, which is formed in the higher catalyst concentration (lower R/C ratio).[40,58,60−62] The density and the shrinkage are not changed obviously when the R/C ratios are between 1000 and 2000. But the higher the R/C ratio (lower catalyst concentration), the larger the pore size and particle size.[40,58,60−62] Thus for the purposes of low shrinkage, low density, and narrow pore size, the R/C and the W/R ratios were set to be 1000 and 16 for preparing the RF sols, which were used to impregnate the PAN fiber felts to prepare composites.

3.2. Textural Properties of the RF Aerogels and the CAs. The pure RF aerogels prepared by R/C ratio of 1000 and W/R ratio of 16 were carbonized to form pure CAs. The nitrogen sorption isotherms, BJH pore size distributions, and SEM images of the RF aerogels and CAs are shown in Figure 4. The RF aerogels and CAs both exhibit a hybrid of type 2 and type 4 isotherms (Figure 4a). Pore size distribution plots show a range of pores extending from the mesoporous to the macroporous regime (Figure 4b), justified the type 4 isotherms. The pore diameter of the peak of the BJH pore size distribution curve of the CA is smaller than that of the RF aerogel, indicative of the shrinkage of the pore during the carbonization process. From the SEM images of the RF aerogels (Figure 4c) and CAs (Figure 4d), it can be seen that both the RF aerogels and the CAs comprise a three-dimensional network of interconnected particles and continuously open macropores, justifying the type 2 isotherms.

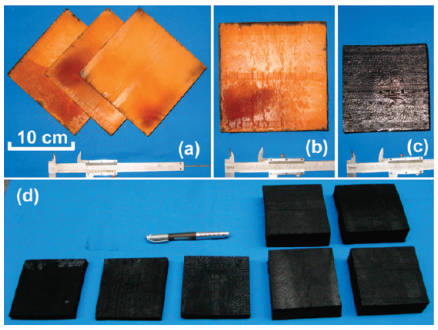

Figure 5. Photographs of (a, b) the PAN/RF aerogel composites and (c, d) the C/CAs. The C/CA in c was derived from the one in b via carbonization and without any further machining. The C/CAs in d had been sawed so they looked smooth on the edges.

The textural properties of the RF aerogels and CAs are shown in Table 1. The densities of the RF aerogels and the CAs are similar, the reason may be the volume shrinkage of approximately 50% and mass loss of 50% during the carbonization process.[41] Both the BET surface area and the pore volume of the RF aerogels are similar to those of CAs. Because of the shrinkage during carbonization, the pore diameters of the peak of the BJH distribution curves decrease from 66 nm for the RF aerogels to 37 nm for the CAs.

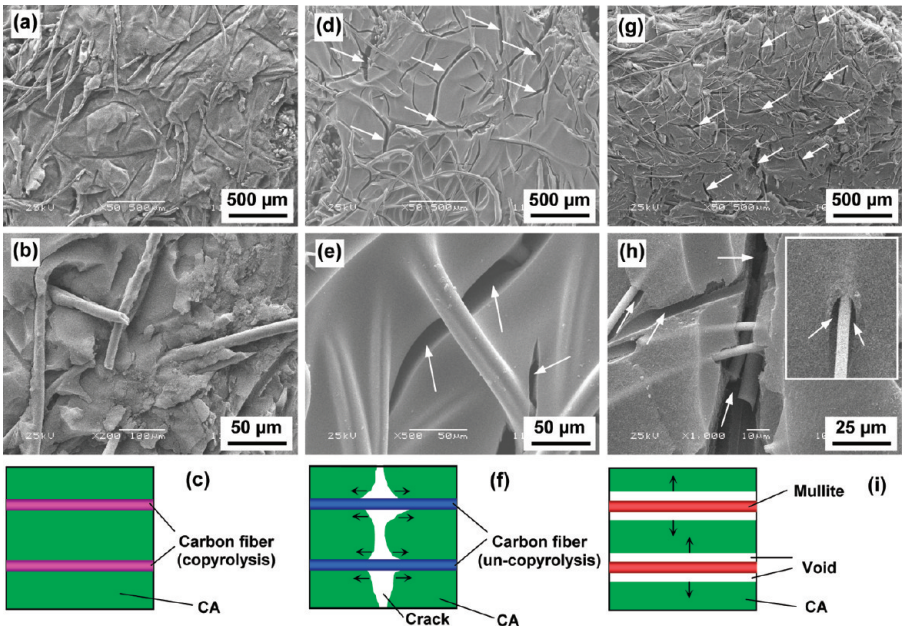

Figure 6. (a) Lower- and (b) higher-magnification SEM images and (c) structure scheme of the C/CAs prepared by copyrolysis of PAN/RF aerogel composites. (d) Lower- and (e) higher-magnification SEM images and (f) crack formation scheme of the C/CAs prepared by carbonizing hard carbon fiber-reinforced RF aerogel composites. (g) Lower- and (h) higher-magnification SEM images and (i) crack formation scheme of the mullite-fiber/CAs. The white arrows in d, e, g, and h indicate the cracks or voids in the CAs. The black arrows in f and i indicate the residual force directions that induce cracks or voids in the CAs. The inset in h shows the void with a diameter larger than that of the mullite fiber.

3.3. Microstructure of the C/CAs. The RF sols prepared by R/C ratio of 1000 and W/R ratio of 16 were used to impregnate the PAN fiber felts (apparent density 0.12 g cm^{-3}), then aged and exchanged with ethanol, and then dried at ambient pressure to obtain organic PAN/RF aerogel composites (0.531 g cm^{-3}). The weight percentage of the oxidized PAN fibers in the PAN/RF aerogel composites is 22.7 wt %. The C/CAs were obtained by carbonizing the organic composites. During the ambient drying process, the linear shrinkage of the composite in the in-plane direction and the through-plane direction are 5.2 and 12.4%, respectively. Because most of the PAN fibers are along the in-plane direction, the shrinkage of the composites in this direction is greatly limited by the fibers, thus the shrinkage (5.2%) is lower than that of the pure RF aerogels (11.0%). While only a few needled fibers are along the through-plane direction, the shrinkage in this direction (12.4%) are much higher than that in the in-plane direction, even a little higher than that of the pure RF aerogels (11.0%). The reason may be the tendency of keeping the volume of the aerogels during the drying process, the lower shrinkage limited by the fibers in the in-plane direction will be equalized by the higher shrinkage in the through-plane direction.

Figure 5 shows the photographs of the PAN/RF aerogel composites and the C/CAs. The color of the oxidized PAN fiber felts is black, after impregnated with the RF aerogels to form composites, the color is yellow (Figure 5a, b). Then the color turns to black after carbonization (Figure 5c, d). The density of the C/CAs is 0.520 g cm^{-3} (porosity 74.9%), which is a little higher than that of the pure CAs (0.446 g cm^{-3}, Table 1), it is attributed to the incorporation of the carbon fibers. The weight percentage of the carbon fibers in the C/CAs is 21.6 wt %. An important feature of the C/CAs is their lack of obvious cracks. This feature ensures low gaseous thermal conductivity and high mechanical strength of the C/CAs, and suggests that the C/CAs can be fabricated in a large-scale setting, which would be important in the thermal insulator applications for thermal protection system. With the PAN fiber-reinforcing and ambient drying method, we easily prepared C/CAs with dimensions of $200 \times 200 \times 35$ mm^3 (see the Supporting Information, Figure s2).

Table 2. Shrinkage and Carbon Yields of the Pure PAN Fibers, Pure RF Aerogels, and Their Composites during the Carbonization Process

materials	in-plane shrinkage (%)	through-plane shrinkage (%)	carbon yield (wt%)
PAN fibers	11.3		51.4
RF aerogels	18.3	18.3	54.7
PAN/RFs	13.2	23.6	54.0

The SEM images of the C/CAs are shown in Figure 6. The SEM images of the composites using carbon fibers and mullite fibers as hard reinforcements are also shown for comparison. There are not any obvious cracks in the C/CAs synthesized by carbonizing the RF aerogel composites with PAN fiber reinforcements (Figure 6a, b). Because the organic PAN fibers shrink with the RF aerogels when the composites are carbonized, it reduces the difference of shrinkage rates between the fiber reinforcements and the aerogel matrices, and thus reduces the residual stresses in the aerogels and then leads to C/CAs without any obvious cracks (Figure 6c). The shrinkage of the pure PAN fiber felts, pure RF aerogels, and their composite during the carbonization process are shown in Table 2. The linear shrinkage of the PAN/RF aerogel composites in the in-plane direction is 13.2%, which is between the value of the pure PAN fiber felts (11.3%) and the value of the pure RF aerogels (18.3%). However, the

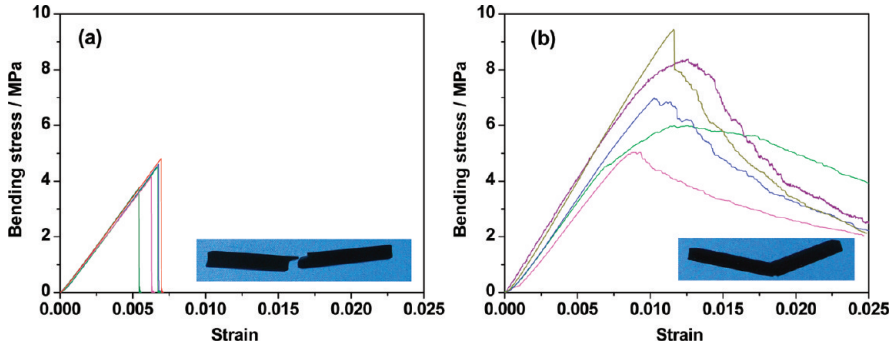

Figure 7. Bending stress versus strain curves (five specimens) of (a) the pure CA and (b) the C/CA. The insets are the pictures of the specimens after three point bending test, the C/CA exhibits fracture toughness and after the test it still joint together by the carbon fibers on the failure point.

linear shrinkage of the PAN/RF aerogel composites in the through-plane direction is 23.6%, which is even higher than that of the pure RF aerogels. The reason may be that the shrinkage of the aerogel in the in-plane direction is limited by the PAN fibers (from 18.3 to 13.2%), thus the shrinkage in the through-plane direction will be higher than that of the pure RF aerogels to keep the volume of the aerogels, it means that the CA matrices in the C/CAs are pulled and elongated in the in-plane direction. Therefore, though the PAN fiber felts shrink with the RF aerogels and thus reducing the residual stresses and avoiding large cracks in the composite, compared to the pure RF aerogels (18.3%), the shrinkage of the pure PAN fiber (11.3%) is still relatively low. In the near future, we will devote our efforts to investigate the shrinkage of other kinds of organic fibers, in order to search out an organic fiber with closer shrinkage to the RF aerogels than the PAN fiber for reinforcements to improve the compatibility between the fibers and the aerogels.

However, there are many cracks in the composites using hard carbon fibers (Figure 6d, e) and mullite fibers (Figure 6g, h) as reinforcements. The cracks are also found in refs 33, 35, and 64. Interestingly, the directions of the cracks in the hard carbon fiber-reinforced composites are different from the ones in the mullite fiber-reinforced composites, we suppose that the reason may be the strong adhesion between the hard carbon fibers and the CAs, and reversely the weak adhesion between the mullite fibers and the CAs. For the hard carbon fiber-reinforced composites, the aerogels shrink but the hard carbon fibers barely shrink, whereas the adhesion on the interface are strong, thus shear stresses are induced in the CAs nearby the interface. The direction of the shear stresses is parallel to the fiber direction (Figure 6f) and induces cracks that are mostly vertical to the fiber direction. However, for the hard mullite fiber-reinforced composites, because of the weak adhesion on the interface, the aerogels split easily on the interface. Thus the direction of the shrink-back force is vertical to the fiber direction (Figure 6i), which induces holes or voids between the mullite fibers and the CAs, and the cracks spread mostly along the fibers. More SEM images indicated the cracks of these two composites can be found in the Supporting Information, Figures s3 and s4.

3.4. Bend Strength and Thermal Conductivity of the C/CA.

Figure 7 shows the bending stress versus strain curves of the pure CA and C/CA. It can be seen that, for the pure CA, the bending stress increases proportionally to the strain and abruptly declines at the highest point when the specimen is broken, this indicates that the pure CA is very brittle. As shown in the inset in Figure 7a, the pure CA ruptured completely into two parts after the three point bending measurement. Although the C/CA is tougher, after the bending stress reaches its highest point, it decreases only gradually with increasing strain, indicative of fracture toughness. The C/CA was not broken completely and was still bridged by the carbon fibers on the failure points (inset in Figure 7b). Overall, the C/CA exhibits higher bend strength of 7.1 ± 1.7 MPa than the pure CA (4.4 ± 0.4 MPa). The improved mechanical properties of the C/CA will be beneficial for load-bearing thermal insulator and also make the material to be easily machined to any possible shapes that required in the thermal protection system. Furthermore, the mechanical properties of the C/CA can be adjusted by adjusting the fiber fraction in the composite.

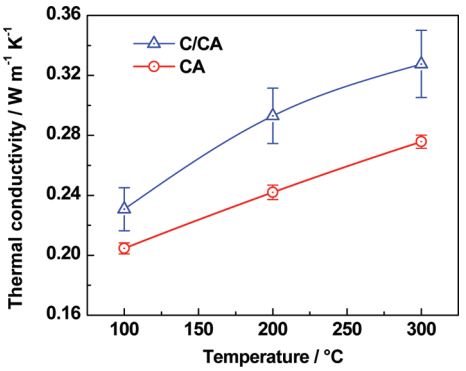

Figure 8. Thermal conductivities of the pure CA specimens (0.446 g cm^{-3}) and the C/CA specimens (0.520 g cm^{-3}) in air by laser flash method. After being reinforced by the carbon fiber via PAN fiber reinforcements, the thermal conductivities of the composite are higher than that of the pure CA, because of the higher solid conductivity attributed to the carbon fiber.

Figure 8 shows the thermal conductivities of the pure CA and the C/CA. It can be seen that the thermal conductivity of the C/CA are higher than that of the pure CA, attributed to the higher solid conductivity of the carbon fiber than that of the pure CA. At 300 °C in air, the thermal conductivity is 0.276 W m^{-1} K^{-1} for the pure CA, and 0.328 W m^{-1} K^{-1} for the C/CA. Actually, the thermal conductivity of the C/CA in this work is higher than that of the low density pure CA (0.066 g cm^{-3}) prepared by supercritical drying in our previous work (0.033 W m^{-1} K^{-1} at 300 °C in air).[65] Nevertheless, the C/CA in this work can be prepared by an easier and lower-cost ambient drying process, and the C/CA exhibits fracture toughness, it is much more robust than the low density pure CA, suggesting

that the C/CA can be more easily handled with and used as load-bearing thermal insulators in inert atmospheres or vacuum.

The characteristic of nanometer pore size of the C/CA can also makes it to be a promising candidate for support material. Silica aerogels and their fiber-reinforced composites have been developed in our laboratory and elsewhere,[23,66,67] and used as supports for phase change materials. It has been concluded that the nanopore of the aerogel can effectively prevent the leakage of the liquid when the phase change materials (paraffin) melt.[66,67] Carbon foam with pore diameters ranging from 200 to 400 μm has also been used by Mesalhy et al. as supports for the phase change materials.[68] It has been concluded that the thermal conductivity of the matrix composite plays an important role in the heat absorption rate. The higher the value of the thermal conductivity of the matrix composite, the higher the value of the heat absorption rate because the high value of thermal conductivity acts to conduct the heat rapidly and acts to absorb heat rapidly.[68] Compared to the silica aerogels, which have very low thermal conductivity (0.013 W m^{-1} K^{-1}),[4] the higher thermal conductivity of the C/CAs in this work will benefit in more rapid heat conduction through the network. Compared to the carbon foam which has micrometer pore diameter, the nanometer pore size of the C/CAs in this work, which is similar to the silica aerogels, will benefit in more effectively preventing leakage of the liquid paraffin. Therefore, the C/CAs can be used as new supports for phase change materials in thermal management. Furthermore, the robust C/CAs can be partially impregnated with phase change materials or phenolic resin to serve as multifunctional materials with multiple properties such as load bearing, thermal insulating, radiation reflecting, and heat absorbing.

In addition, our organic fiber-reinforced composites are not limited by using base-catalyst RF aerogels as matrices. The similar raw materials, that do not need oxidation and can be dried at ambient pressure, can also be used as the matrices, such as phenol-furfural, resorcinol-furfural, phenol-formaldehyde, and polyimide aerogels. Even the oxidized PAN fiber reinforcements can be replaced by other organic fibers that can be carbonized to form carbon fibers compatible with the organic aerogels. We think this flexibility is an advantage of our method.

4. CONCLUSIONS

A new C/CA architecture was prepared by ambient drying and copyrolysis of organic fiber-reinforced organic aerogel composite. Upon carbonization the organic PAN fibers shrink with the RF aerogels, thus reducing the difference of the shrinkage rates between the fiber reinforcements and the aerogel matrices, and thus reducing the residual stresses, and then leading to C/CA without any obvious cracks. The C/CA exhibits fracture toughness, it has higher bend strength and higher thermal conductivity than the pure CA. Further optimization of the controllable parameters of the C/CAs is expected to produce composites with even greater properties for special use as extremely high-temperature thermal insulators in inert atmospheres or vacuum, or phase change material supports. Together with the easy handling, resulting from the improved mechanical properties, the lack of obvious cracks, and the ease of fabrication, our new method may lead to lower-cost and larger scale industrial processes, suggesting that CAs will find increased usage in thermal management applications.

■ ASSOCIATED CONTENT

Supporting Information. Detailed laser flash measurement mechanism and process, photographs of the carbon aerogel composite and the specimens for thermal diffusivity and three point bending measurements, and additional SEM images of the composites using hard carbon fibers and mullite fibers as reinforcements. This material is available free of charge via the Internet at http://pubs.acs.org.

■ AUTHOR INFORMATION

Corresponding Author
*E-mail: fengj@nudt.edu.cn.

■ ACKNOWLEDGMENT

This work was supported by the National Natural Science Foundation (51002187, 51172279) and the National Defense Preliminary Research Foundation (9140C8203051003) of China. The authors thank Prof. Zengyong Chu for discussion and proofreading the paper, and Dr. Meng Liu for laser flash measurements.

■ REFERENCES

(1) Huang, W.; Qin, H.; Luo, S. B.; Wang, Z. G. *Sci. China Tech. Sci.* **2010**, *53*, 220–226.
(2) Glass, D. E. Ceramic Matrix Composite (CMC) Thermal Protection Systems (TPS) and Hot Structures for Hypersonic Vehicles. Presented at the 15th AIAA International Space Planes and Hypersonic Systems and Technologies Conference; AIAA: Reston, VA, 2008; AIAA-2008-2682.
(3) Pierre, A. C.; Pajonk, G. M. *Chem. Rev.* **2002**, *102*, 4243–4265.
(4) Lu, X.; Arduini-Schuster, M. C.; Kuhn, J.; Nilsson, O.; Fricke, J.; Pekala, R. W. *Science* **1992**, *255*, 971–972.
(5) Randall, J. P.; Meador, M. A. B.; Jana, S. C. *ACS Appl. Mater. Interfaces* **2011**, *3*, 613–626.
(6) Baumann, T. F.; Gash, A. E.; Chinn, S. C.; Sawvel, A. M.; Maxwell, R. S.; Satcher, J. H., Jr. *Chem. Mater.* **2005**, *17*, 395–401.
(7) Chervin, C. N.; Clapsaddle, B. J.; Chiu, H. W.; Gash, A. E.; Satcher, J. H., Jr.; Kauzlarich, S. M. *Chem. Mater.* **2005**, *17*, 3345–3351.
(8) Meador, M. A. B.; Weber, A. S.; Hindi, A.; Naumenko, M.; McCorkle, L.; Quade, D.; Vivod, S. L.; Gould, G. L.; White, S.; Deshpande, K. *ACS Appl. Mater. Interfaces* **2009**, *1*, 894–906.
(9) Bigall, N. C.; Herrmann, A. K.; Vogel, M.; Rose, M.; Simon, P.; Carrillo-Cabrera, W.; Dorfs, D.; Kaskel, S.; Gaponik, N.; Eychmüller, A. *Angew. Chem., Int. Ed.* **2009**, *48*, 9731–9734.
(10) Korhonen, J. T.; Kettunen, M.; Ras, R. H. A.; Ikkala, O. *ACS Appl. Mater. Interfaces* **2011**, *3*, 1813–1816.
(11) Leventis, N.; Sotiriou-Leventis, C.; Chandrasekaran, N.; Mulik, S.; Larimore, Z. J.; Lu, H. B.; Churu, G.; Mang, J. T. *Chem. Mater.* **2010**, *22* 6692–6710.
(12) Zou, J. H.; Liu, J. H.; Karakoti, A. S.; Kumar, A.; Joung, D.; Li, Q.; Khondaker, S. I.; Seal, S.; Zhai, L. *ACS Nano* **2010**, *4*, 7293–7302.
(13) Li, L.; Yalcin, B.; Nguyen, B. N.; Meador, M. A. B.; Cakmak, Miko. *ACS Appl. Mater. Interfaces* **2009**, *1*, 2491–2501.
(14) Guo, H.; Meador, M. A. B.; McCorkle, L.; Quade, D. J.; Guo, J.; Hamilton, B.; Cakmak, M.; Sprowl, G. *ACS Appl. Mater. Interfaces* **2011**, *3*, 546–552.
(15) Worsley, M. A.; Pauzauskie, P. J.; Olson, T. Y.; Biener, J.; Satcher, J. H., Jr.; Baumann, T. F. *J. Am. Chem. Soc.* **2010**, *132* 14067–14069.
(16) Lin, Y.; Ehlert, G. J.; Bukowsky, C.; Sodano, H. A. *ACS Appl. Mater. Interfaces* **2011**, *3*, 2200–2203.
(17) Hanzawa, Y.; Hatori, H.; Yoshizawa, N.; Yamada, Y. *Carbon* **2002**, *40*, 575–581.

(18) Wiener, M.; Reichenauer, G.; Hemberger, F.; Ebert, H. P. *Int. J. Thermophys.* **2006**, *27*, 1826–1843.
(19) Baxter, R. I.; Rawlings, R. D.; Iwashita, N.; Sawada, Y. *Carbon* **2000**, *38*, 441–449.
(20) Feng, J.; Feng, J.; Jiang, Y.; Zhang, C. *Mater. Lett.* **2011**, *65* 3454–3456.
(21) Meador, M. A. B.; Scherzer, C. M.; Vivod, S. L.; Quade, D.; Nguyen, B. N. *ACS Appl. Mater. Interfaces* **2010**, *2*, 2162–2168.
(22) Nguyen, B. N.; Meador, M. A. B.; Tousley, M. E.; Shonkwiler, B.; McCorkle, L.; Scheiman, D. A.; Palczer, A. *ACS Appl. Mater. Interfaces* **2009**, *1*, 621–630.
(23) Meador, M. A. B.; Vivod, S. L.; McCorkle, L.; Quade, D.; Sullivan, R. M.; Ghosn, L. J.; Clark, N.; Capadona, L. A. *J. Mater. Chem.* **2008**, *18*, 1843–1852.
(24) Nguyen, B. N.; Meador, M. A. B.; Medoro, A.; Arendt, V.; Randall, J.; McCorkle, L.; Shonkwiler, B. *ACS Appl. Mater. Interfaces* **2010**, *2*, 1430–1443.
(25) Leventis, N.; Sotiriou-Leventis, C.; Zhang, G.; Rawashdeh, A.-M. M. *Nano Lett.* **2002**, *2*, 957–960.
(26) Leventis, N.; Mulik, S.; Sotiriou-Leventis, C. *Chem. Mater.* **2008**, *20*, 6985–6997.
(27) Luo, R.; Liu, T.; Li, J.; Zhang, H.; Chen, Z.; Tian, G. *Carbon* **2004**, *42*, 2887–2895.
(28) Ma, Y.; Wang, S.; Chen, Z. H. *Carbon* **2011**, *49*, 2869–2872.
(29) Chen, S.; Hu, H.; Zhang, Y.; He, X.; Mei, M. *Mater. Lett.* **2011**, *65*, 3137–3139.
(30) Liu, H.; Cheng, H.; Wang, J.; Tang, G.; Che, R.; Ma, Q. *Mater. Sci. Eng., A* **2009**, *525*, 121–127.
(31) Wang, H.; Zhou, X.; Yu, J.; Cao, Y.; Liu, R. *Mater. Lett.* **2010**, *64* 1691–1693.
(32) Schmitt, C.; Pröbstle, H.; Fricke, J. *J. Non-Cryst. Solids* **2001**, *285*, 277–282.
(33) Drach, V.; Wiener, M.; Reichenauer, G.; Ebert, H.-P.; Fricke, J. *Int. J. Thermophys.* **2007**, *28*, 1542–1562.
(34) Fu, R.; Zheng, B.; Liu, J.; Weiss, S.; Ying, J. Y.; Dresselhaus, M. S.; Dresselhaus, G.; Satcher, J. H., Jr.; Baumann, T. F. *J. Mater. Res.* **2003**, *18*, 2765–2773.
(35) Bordjiba, T.; Mohamedi, M.; Dao, L. H. *Adv. Mater.* **2008**, *20* 815–819.
(36) Liu, T.; Sreekumar, T. V.; Kumar, S.; Hauge, R. H.; Smalley, R. E. *Carbon* **2003**, *41*, 2440–2442.
(37) Worsley, M. A.; Satcher, J. H., Jr.; Baumann, T. F. *Langmuir* **2008**, *24*, 9763–9766.
(38) Gutièrrez, M. C.; Rubio, F.; Monte, F. *Chem. Mater.* **2010**, *22* 2711–2719.
(39) Yang, J.; Li, S.; Luo, Y.; Yan, L.; Wang, F. *Carbon* **2011**, *49* 1542–1549.
(40) Feng, J.; Feng, J.; Zhang, C. *J. Sol−Gel Sci. Technol.* **2011**, *59*, 371–380.
(41) Al-Muhtaseb, S. A.; Ritter, J. A. *Adv. Mater.* **2003**, *15*, 101–114.
(42) Gupta, A.; Harrison, I. R. *Carbon* **1997**, *35*, 809–818.
(43) Qin, X.; Lu, Y.; Xiao, H.; Hao, Y.; Pan, D. *Carbon* **2011**, *49* 4598–4600.
(44) Albert, D. F.; Andrews, G. R.; Mendenhall, R. S.; Bruno, J. W. *J. Non-Cryst. Solids* **2011**, *296*, 1–9.
(45) Biesmans, G.; Mertens, A.; Duffours, L.; Woignier, T.; Phalippou, J. *J. Non-Cryst. Solids* **1998**, *225*, 64–68.
(46) Leventis, N.; Sotiriou-Leventis, C.; Chandrasekaran, N.; Mulik, S.; Larimore, Z. J.; Lu, H.; Churu, G.; Mang, J. T. *Chem. Mater.* **2010**, *22* 6692–6710.
(47) Lorjai, P.; Chaisuwan, T.; Wongkasemjit, S. *J. Sol−Gel Sci. Technol.* **2009**, *52*, 56–64.
(48) Katanyoota, P.; Chaisuwan, T.; Wongchaisuwat, A.; Wongkasemjit, S. *Mater. Sci. Eng., B* **2010**, *167*, 36–42.
(49) Bordjiba, T.; Mohamedi, M.; Dao, L. H. *J. Power Sources* **2007**, *172*, 991–998.
(50) Reuß, M.; Ratke, L. *J. Sol−Gel Sci. Technol.* **2008**, *47*, 74–80.
(51) Mulik, S.; Sotiriou-Leventis, C.; Leventis, N. *Chem. Mater.* **2007**, *19*, 6138–6144.
(52) Leventis, N.; Chandrasekaran, N.; Sadekar, A. G.; Mulik, S.; Sotiriou-Leventis, C. *J. Mater. Chem.* **2010**, *20*, 7456–7471.
(53) Aegerter, M. A.; Leventis, N.; Koebel, M. M. *Aerogels Handbook*; Springer: New York, 2011; pp215−234.
(54) Reichenauer, G.; Stumpf, C.; Fricke, J. *J. Non-Cryst. Solids* **1995**, *186*, 334–341.
(55) Xiang, J.; Drzal, L. T. *Carbon* **2011**, *49*, 773–778.
(56) Veca, L. M.; Meziani, M. J.; Wang, W.; Wang, X.; Lu, F.; Zhang, P.; Lin, Y.; Fee, R.; Connell, J. W.; Sun, Y. P. *Adv. Mater.* **2009**, *21* 2088–2092.
(57) Wiener, M.; Reichenauer, G.; Braxmeier, S.; Hemberger, F.; Ebert, H. P. *Int. J. Thermophys.* **2009**, *30*, 1372–1385.
(58) Job, N.; Théry, A.; Pirard, R.; Marien, J.; Kocon, L.; Rouzaud, J. N.; Béguin, F.; Pirard, J.-P. *Carbon* **2005**, *43*, 2481–2494.
(59) Fidalgo, A.; Farinha, J. P. S; Martinho, J. M. G.; Rosa, M. E.; Ilharco, L. M. *Chem. Mater.* **2007**, *19*, 2603–2609.
(60) Zhu, Y.; Hu, H.; Li, W.; Zhao, H. *J. Non-Cryst. Solids* **2006**, *352* 3358–3362.
(61) Lee, Y. J.; Jung, J. C.; Yi, J.; Baeck, S.-H.; Yoon, J. R.; Song, I. K. *Curr. Appl. Phys.* **2010**, *10*, 682–686.
(62) Wu, D.; Fu, R. *J. Porous Mater.* **2008**, *15*, 29–34.
(63) Brandt, R.; Fricke, J. *J. Non-Cryst. Solids* **2004**, *350*, 131–135.
(64) Talbi, H.; Just, P.-E.; Dao, L. H. *J. Appl. Electrochem.* **2003**, *33* 465–473.
(65) Feng, J.; Feng, J.; Zhang, C. *J. Porous Mater.* **2011**, doi: 10.1007/s10934-011-9504-7.
(66) Zhou, X.; Xiao, H.; Feng, J.; Zhang, C.; Jiang, Y. *Compos. Sci. Technol.* **2009**, *69*, 1246–1249.
(67) Zhou, X.; Xiao, H.; Feng, J.; Zhang, C.; Jiang, Y. *Chem. Eng. Res. Des.* **2010**, *88*, 1013–1017.
(68) Mesalhy, O.; Lafdi, K.; Elgafy, A. *Carbon* **2006**, *44*, 2080–2088.